ALGORITHM AND DATA USER MANUAL FOR THE SPECIAL SENSOR MICROWAVE IMAGER/ SOUNDER (SSMIS)

Appendix A: SSMIS BEAM LOCATION ALGORITHM

Northrop Grumman
Contract No: F04710-00-C-0001

TECHNICAL REPORT

Prepared by:

Northrop Grumman Corporation
Space Systems Division
1100 West Hollyvale Street
Post Office Box 296
Azusa, California 91702-0296

TABLE OF CONTENTS

SECTION **Page**

FIGURES

TABLES

Editor's note: Acknowledgement and appreciation is given to Alex Stogryn for providing the information in this Appendix.

1 SSMIS BEAM LOCATION ALGORITHM

This appendix discusses the mathematical approach for the SSMIS beam location algorithm.

1.1 Introduction and summary

The requirements for the SSMIS state that atmospheric profiles from the 1000 mb level to the 10 mb level shall be referenced to a height of 11 km and shall be located with an accuracy of 12.5 km. The earth location of upper air temperature profiles from the 7 mb level to the 0.03 mb level shall be referenced to a height of 60 km, and shall be accurate to 12.5 killometers. The other environmental parameters shall be Earth located to within 7 km (at the Earth's surface).

The SSMIS is a 24-channel instrument which, for purposes of a location algorithm, may be described in terms of 180 basic beam positions forming a swath generated by scanning the radiometer antenna. With respect to a satellite fixed coordinate system, the basic beams lie on the surface of a cone with a 45° half angle whose axis is in the direction of the subsatellite Earth normal vector. The centers of the beams are separated by an azimuthal angle of exactly 0.8°.

For those channels whose frequencies exceed 91 GHz, all 180 beam positions are used to generate fine resolution imagery. Inputs into the atmospheric profiling algorithms for levels up to 10 mb are formed by averaging 9 of the basic beams, 3 along the scan direction x 3 successive scans. This results in 60 beams per scan (starting from basic beam position 2 and separated from each other by an azimuthal angle of 2.4°) every third scan line. To form input to the upper air temperature profiling algorithm, six along-scan samples are averaged resulting in 30 samples (spaced 4.8° apart) every 6^{th} scan. For the channels used for retrieving non-sounding parameters with frequencies in the 19 to 37 GHz range, the required integration time is twice that of the basic beam integration time so that a total of 90 of these beams, with centers separated by an azimuthal angle of 1.6°, are formed per scan.

The preceding description shows that three categories of locations are required. The first is the location of the 180 basic beams per scan at the Earth's surface. The second is the location of 60 beams every third scan at a height of 11 km. And the third is the location of 30 beams every 6^{th} scan at a height of 60 km. The locations of the low frequency (19 to 37 GHz) beams are found simply by averaging the coordinates of the two basic beams that cover a single low frequency beam.

Since well over one-half million beams will be located per orbit if every beam is processed, it is clear that care must be exercised in constructing an efficient algorithm. The exact location of every beam in a scan requires a large number of computer operations and, hence, is not a desirable procedure. Thus, following the method used for the SSM/I, only certain points (referred to as base points), are located exactly. The others are located by means of third degree interpolatory polynomials. However, the SSM/I algorithm cannot be assumed to apply directly to the SSMIS because

a. The SSMIS swath width is much larger. Thus, the number of base points required to achieve the specified accuracy must be redetermined.

b. The SSM/I algorithm references beams to the surface only. It must be re-worked to include other reference heights.

In view of the fact that changes were required in the SSM/I location algorithm, it was decided to make a thorough revision. This resulted in accuracy improvements in locating the base points by use of concepts developed for the SSM/T-2. An improvement in the interpolatory accuracy between the base points was achieved by exploiting the fact that the base points do not have to be equally spaced in azimuth. Savings were made in the number of operations (evaluations of transcendental functions, multiplication, division, etc.) needed to locate the base points by using techniques developed for the SSM/T-2. Further, great savings were made in the operations count for determining the interpolated beam positions by developing a new algorithm that does not explicitly calculate the coefficients of the interpolatory polynomials but fully exploits the fact that the beams are equally spaced in azimuthal angle.

The resulting SSMIS beam location algorithm, like that used for the SSM/I, determines a full scan of beam positions once a given scan is targeted for location. Even though considerably more than the 128 beam positions per scan applicable to the SSM/I are located, the SSMIS algorithm is faster due to the improvements made. The accuracy is superior. Ignoring deviations from non-ideal behavior such as radiometer mounting misalignment, spacecraft attitude misalignment, and possible errors in predicted ephemeris data, the maximum beam location error found using the SSMIS algorithm is less than 2.7 km for a nominal 833 km (450 nm) orbit. This occurs at high latitudes. Considerably smaller errors are found in tropic and temperate regions. As for the effects of non-ideal behavior, provision is made in the algorithm to accommodate alignment effects as they are discovered. Only analyzing the final mechanical design and/or using in-flight data, of course, can make these.

1.2 Basic equations

For an ellipsoidal model Earth, the Earth's surface may be described by the equation

$$\frac{x^2 + y^2}{A^2{}_e} + \frac{z^2}{A_p^2} = 1$$

Eq. 1

where A_e = 6378.165 km is the equatorial radius and A_p = 6356.788 km is the polar radius (see Figure 1). By taking the gradient of (Eq. 1), it is readily found that the unit normal to the surface at the point (x, y, z) is given by the vector

$$\hat{n} = \left(x, y, \left(\frac{A_e}{A_p} \right)^2 z \right) F_n(z)$$

Eq. 2

where

$$F_n(z) = \left[A_e \left\{ 1 + \frac{A_e^2 - A_p^2}{A_p^2} \frac{z^2}{A_p^2} \right\}^{1/2} \right]^{-1}$$

Eq. 3

A point on the surface is often described by means of its longitude defined as

$$\phi = \tan^{-1}\left(\frac{n_y}{n_x}\right)$$

Eq. 4

and latitude λ defined as

$$\lambda = \tan^{-1}\left(n_z / \sqrt{n_x^2 + n_y^2}\right)$$

Eq. 5

Notice that the latitude does not coincide with the angle θ of the radius vector from the center of the Earth (Figure 1). The rectangular coordinates of a point are expressed in terms of these parameters as

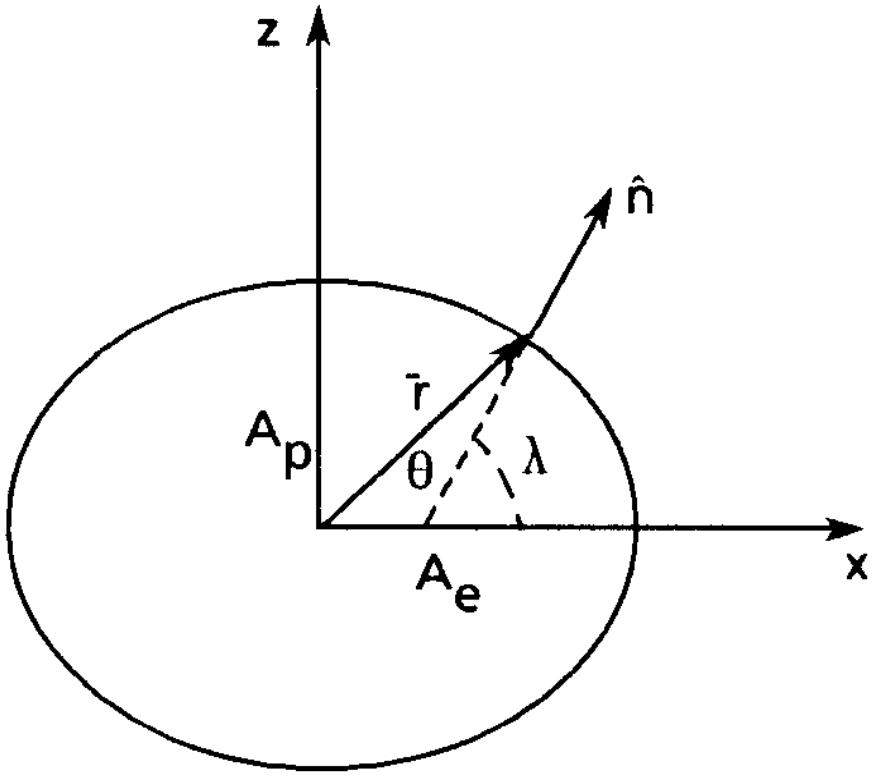

Figure 1. Ellipsoidal Earth Geometry

$$y = \left(\frac{A_e}{A_p} \right)^2 \cos\lambda \sin\phi F_Z(\lambda)$$

$$x = \left(\frac{A_e}{A_p} \right)^2 \cos\lambda \cos\phi F_Z(\lambda)$$

$$z = \sin\lambda F_Z(\lambda)$$

Eq. 6

where

$$F_z(\lambda) = A_p^2 \left[A_e^2 \cos^2\lambda + A_p^2 \sin^2\lambda \right]^{1/2}$$

Eq. 7

Here the z-axis points from the center of the Earth to the north pole and the x-axis from the center of the Earth to the equator at 0° longitude.

In order to use these equations to locate a beam, it is necessary to know the location of the satellite, its orientation, and the beam vector. It may be assumed that the subsatellite latitude and longitude and the satellite height are known at two distinct times t_1 and t_2 where t_1 is typically one minute less than t_2. Because the Earth rotates, one must be careful to express all quantities in the same coordinate system fixed in space which, in this note, will be taken to be the Earth fixed frame at time t_2. Thus, the vector to the subsatellite point at time t_2 is

$$\bar{r}_2 = (x_2, y_2, z_2)$$

Eq. 8

where x_2, y_2 and z_2 are given by (Eq. 6) using subsatellite latitude and longitude values λ_2 and ϕ_2. If the subsatellite latitude and longitude are λ_{ss} and ϕ_{ss} at time t_1, then the vector to the subsatellite point at time t_1 is expressed in the space fixed frame as

$$\bar{r}_1 = (x_1, y_1, z_1)$$

Eq. 9

where equations (Eq. 6) are used again, but with latitude and longitude values

Error! Objects cannot be created from editing field codes.

Error! Objects cannot be created from editing field codes.

Eq. 10

substituted for λ and ϕ. Here Ω is the angular speed of the Earth (= 7.2921159 x 10^{-5} rad/sec). Since the satellite height is measured along the normal from the surface, the satellite position is given as

$$\bar{r}_{s2} = \bar{r}_2 + h(t_2)\,\hat{n}_2$$

$$\bar{r}_{s1} = \bar{r}_1 + h(t_1)\,\hat{n}_1$$

Eq. 11

where h(t) is the height, $\bar{r}_2$ and $\bar{r}_1$ are given by (Eq. 8) and (Eq. 9), and $\hat{n}_2$ and $\hat{n}_1$, are given by (Eq. 2) with subscript either 2 or 1 on the coordinates. A unit vector perpendicular to the orbit plane between times t_1 and t_2 is

$$\hat{x}_s = \bar{r}_{s2} \times \bar{r}_{s1} / \left| \bar{r}_{s2} \times \bar{r}_{s1} \right|$$

Eq. 12

Given the above data, it is possible to find approximate equations for the satellite and beam (in the space fixed reference frame) at some time t in the interval $t_1 \le t \le t_2$. First, one can show that if it is assumed that the Earth is a sphere instead of an ellipsoid and that the satellite angular speed □ is constant between the times t_2 and t_1, then the sub-satellite vector at time t is

$$\bar{r}(t) = -\frac{\sin\omega(t - t_2)}{\sin\omega(t_2 - t_1)}\bar{r}_1 + \frac{\sin\omega(t - t_1)}{\sin\omega(t_2 - t_1)}\bar{r}_2$$

Eq. 13

In reality, the Earth is not a sphere and the angular speed is not necessarily a constant. However, (Eq. 13) may be applied with ω representing the average speed. This is generally a very good approximation for $t_2 - t_1$ of the order of a minute. Further, (Eq. 13) is exact at times t_1 and t_2 for the true ellipsoid Earth and introduces only a small error for other times t if $t_2 - t_1$ is small. This same approximation is also very suitable for the unit normal $\hat{n}(t)$ as is evident from (Eq. 2) and (Eq. 3). Notice, in this connection, that F_n is nearly a constant over a small time interval because z will not change much. Thus, the equation

$$\hat{n}(t) = -\frac{\sin\omega(t - t_2)}{\sin\omega(t_2 - t_1)}\hat{n}_1 + \frac{\sin\omega(t - t_1)}{\sin\omega(t_2 - t_1)}\hat{n}_2$$

Eq. 14

is obtained. Further, since the satellite orbit is assumed to be nearly circular, the same arguments lead to the equation

$$\bar{r}_s(t) = -\frac{\sin\omega(t - t_2)}{\sin\omega(t_2 - t_1)}\bar{r}_{s1} + \frac{\sin\omega(t - t_1)}{\sin\omega(t_2 - t_1)}\bar{r}_{s2}$$

Eq. 15

for the vector to the satellite at time t in the space fixed frame.

The preceding equations must be supplemented by data on the beam direction in order to compute the beam location on the Earth. Beam directions are defined with respect to spacecraft coordinates. Taking the vectors $\hat{n}(t)$ and $\hat{x}(t)$ as defining two spacecraft fixed vectors, a third vector is

$$\hat{y}_s(t) = \hat{n}(t) \times \hat{x}_s$$

Eq. 16

Eq. 17 was omitted in original document. (Note that $\hat{y}_s(t)$ would be parallel to the velocity if the orbit were exactly circular and the difference between $\hat{n}$ and a unit vector from the center of the Earth to the spacecraft could be ignored). Since $\hat{x}_s$ is a constant, (Eq. 14) shows that $\hat{y}_s(t)$ may be expressed as

$$\hat{y}_s(t) = -\frac{\sin\omega\cdot(t-t_2)}{\sin\omega\cdot(t_2-t_1)}\,\hat{y}_{s1} + \frac{\sin\omega\cdot(t-t_1)}{\sin\omega\cdot(t_2-t_1)}\,\hat{y}_{s2}$$

Eq. 18

where the constant vectors $\hat{y}_{s1}$ and $\hat{y}_{s2}$ are defined as

$$\hat{y}_{s1} = \hat{n}(t_1) \times \hat{x}_s$$

Eq. 19

$$\hat{y}_{s2} = \hat{n}(t_2) \times \hat{x}_s$$

Eq. 20

For a conical scan, the unit vector $\hat{s}$ along the beam direction is

$$\hat{s} = \sin\psi\cos\phi_s(t)\hat{x}_s + \sin\psi\sin\phi_s(t)\hat{y}_s(t) - \cos\psi\hat{n}(t)$$

Eq. 21

where ψ is the cone angle and $\phi_s(t)$ the azimuthal angle of the beam as is illustrated in Figure 2. For the SSMIS, the scan rate is 31.6 rpm and the initial basic beam position in a scan is at 198.4°. Thus, at the time t in a scan beginning at time t_s,

$$\phi_s(t) = 198.4 + 189.6(t - t_s)$$

Eq. 22

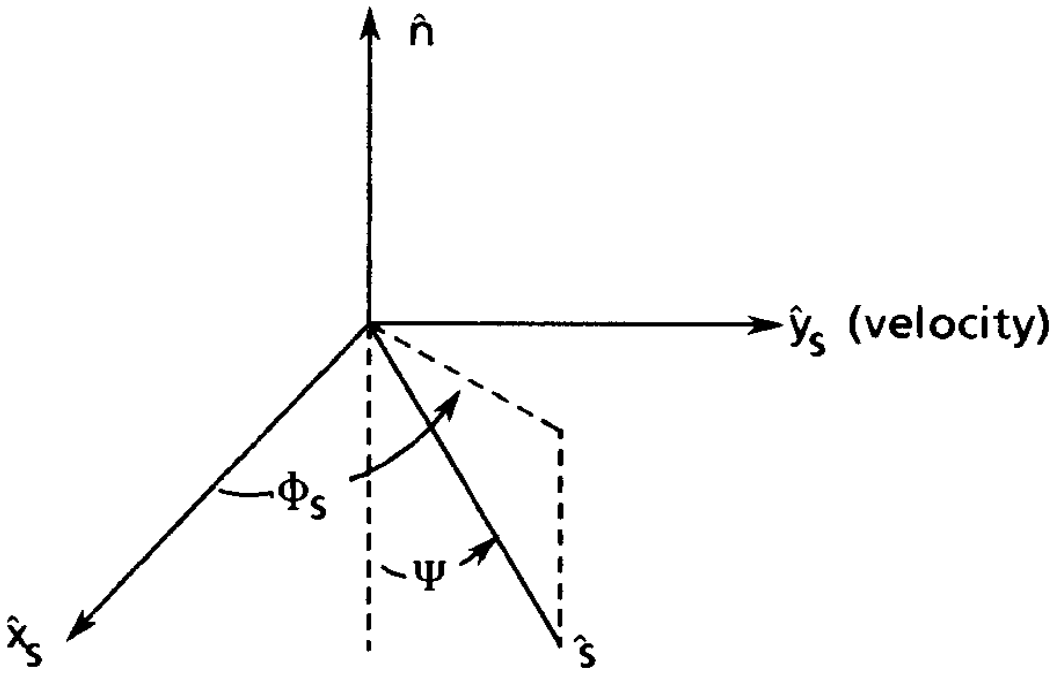

Figure 2. Beam Direction Geometry

where t and t_s are in seconds and $\phi_s(t)$ in degrees.

If the slant range to the Earth is s, as shown in Figure 3,

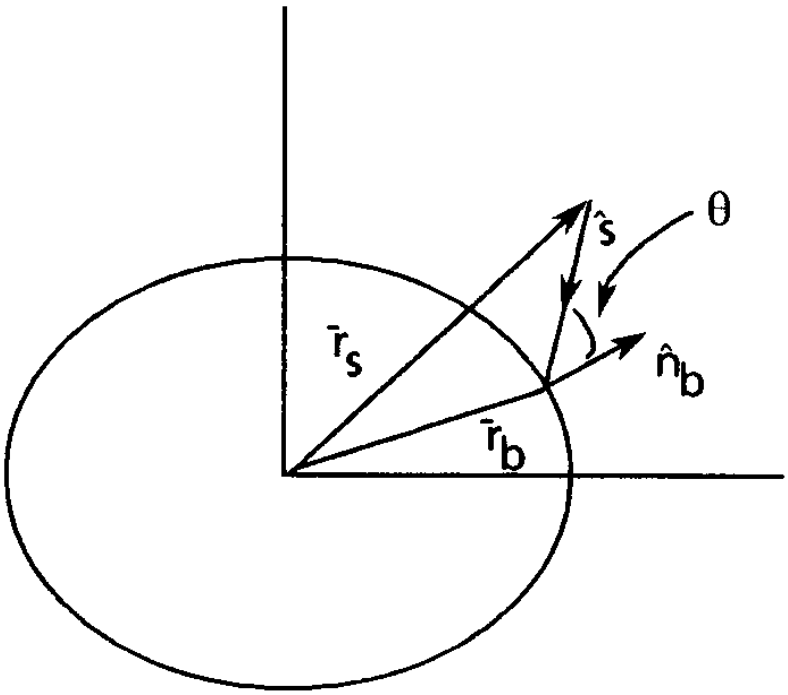

Figure 3. Beam Location Geometry

then the beam intersects the Earth at the point

$$\bar{r}_b(t) = \bar{r}_s(t) + s\,\hat{s}$$

Eq. 23

The range s is determined by the condition that the components of $\bar{r}_b(t)$ must satisfy (Eq. 1). This leads to a quadratic equation for s. Choosing the solution that lies on the side of the Earth which is visible from the satellite yields

$$s = -\left(\beta + \sqrt{\beta^2 - \alpha\gamma}\right)/\alpha$$

Eq. 24

where

$$\alpha = 1 + a^2 s_z^2$$

Eq. 25

$$\beta = \bar{r}_s(t) \bullet \hat{s} + a^2 z_s s_z$$

Eq. 26

$$\gamma = \left|\bar{r}_s(t)\right|^2 + a^2 z_s^2 - A_e^2$$

Eq. 27

and a is the constant $[A_e^2 - A_P^2]^{1/2}/A_P = 8.207943 \times 10^{-2}$. Here z_s and s_z are the z components of $\bar{r}_s(t)$ and $\hat{s}$, respectively.

With s computed as above, the beam latitude and longitude are immediately found from (Eq. 22) and (Eq. 6) as

$$(\lambda_b)_{t2} = \tan^{-1}\left[\left(\frac{A_e}{A_p}\right)^2 \frac{z_b}{\sqrt{x_b^2 + y_b^2}}\right]$$

Eq. 28

$$(\phi_b)_{t2} = \tan^{-1}\frac{y_b}{x_b}$$

Eq. 29

These equations, of course, refer to the space fixed coordinate frame. A transformation to the standard Earth fixed frame at time t yields

$$\lambda_b = (\lambda_b)_{t_2}$$

Eq. 30

$$\phi_b = (\phi_b)_{t_2} + \Omega \cdot (t_2 - t)$$

Eq. 31

This completes the derivation of the equations for locating a beam at the Earth's surface.

If the beam is referenced to a height h_R, then (Eq. 23) must be replaced by

$$\bar{r}_b = \bar{r}_s + s\,\hat{s} - h_R \hat{n}_b$$

Eq. 32

where $\hat{n}_b$ is the unit Earth normal at the beam position $\bar{r}_b$ (see Figure 4). By use of (Eq. 2), (Eq. 32) and (Eq. 1) becomes a set of four scalar equations for the four unknowns x_b, y_b, z_b, and s. This set of non-linear equations must be solved numerically. While this procedure is exact, it is not practical for an operational algorithm and is mainly of interest for checking approximations. Later, a simple modification to (Eq. 24) will be shown to lead to an accurate and practical numerical procedure for operational use.

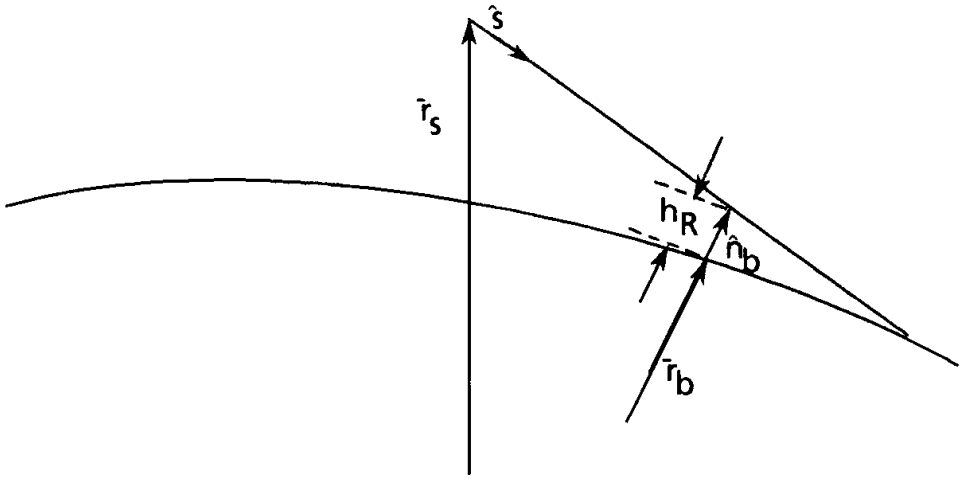

Figure 4. Beam Location for Non-Zero Reference Height - hR

1.3 Numerical considerations

A computer program using the basic equations discussed in Section 1.2, while accurate, would result in a very computational intensive procedure for locating the SSMIS beams. In this section, a number of approximations that will allow a fast computation of beam locations will be considered. It will be assumed that ephemeris data (subsatellite latitude and longitude and satellite altitude at a known time) will be available in approximately one-minute intervals. Further, the assumption is made that, if a given scan is targeted for analysis, all beam locations in that scan will be found.

Section 1.3.1 discusses the computation of quantities depending only on the ephemeris data. To locate a beam, the beam direction (including angles describing possible misalignment) must be specified. Section 1.3.2 discusses equations for the beam direction. This is followed in Section 1.3.3 by a discussion of a simple, accurate method for treating the problem of the variable reference heights that will be specified for beam locations.

Even with the simplifications introduced in these sections, the location of every beam in a scan would lead to a massive computational problem without further approximation. For this reason, only certain base points (not necessarily coinciding with real beam centers, as described below) are located precisely. The location of these base points is treated in Section 1.3.4. An interpolation method for locating the beams using these base points is discussed in Section 1.3.5 where it is shown that increased location accuracy is achieved by a non-uniform spacing of the base points without incurring any computational penalties. The interpolating scheme for locating the beam passes two third-degree polynomials (one for the latitude and one for the longitude) between sets of four successive base point coordinates. These polynomials, however, are not defined explicitly. Instead, a very efficient recursive method, which after initializing some auxiliary variables, requires only three additions per polynomial evaluation, is possible because of the equal azimuthal angle spacing between beams in a given scan line.

1.3.1 Ephemeris computations

The starting point for a beam location is the subsatellite latitude and longitude at two times t_1 and t_2. This information must be converted to rectangular coordinate data for use in (Eq. 11), which defines the vectors to the satellite. It is not possible to bypass the computations of the trigonometric functions occurring in (Eq. 6) for the subsatellite vector. However, the remainder of the computation involving the functions F_n and F_z (see (Eq. 3) and (Eq. 7)) can be simplified considerably. An expansion in Chebychev polynomials and subsequent truncation of the series show that

$$F_z(\lambda) = 6356.775 - 21.305\cos^2\lambda \ \text{km}$$

Eq. 33

with an error less than 0.014 km while

$$F_n(z) = 1.5678457\text{x}10^{-4} - 1.3004\text{x}10^{-14}z^2 \ \text{km}^{-1}$$

Eq. 34

(where z is expressed in km) with an error less than 3.32×10^{-10} km^{-1} if the values for A_e and A_p given in connection with (Eq. 1) are used.

The next quantity that is used is $\hat{x}_s$ defined in (Eq. 12). In evaluating the vector cross product, it is useful to observe that $\bar{r}_{S1}$ and $\bar{r}_{S2}$ are nearly parallel. Thus $\bar{r}_{S2} \times \bar{r}_{S1}$ will be a small quantity. In order to avoid multiplying large numbers and relying on cancellation as subtractions are performed in computing $\bar{r}_{S2} \times \bar{r}_{S1}$, it is numerically preferable to evaluate this as

$$\bar{r}_{s2} \times \bar{r}_{s1} = \left(\bar{r}_{s2} - \bar{r}_{s1}\right) \times \bar{r}_{s2}$$

Eq. 35

The bracket in (Eq. 35) is already small (and nearly perpendicular to $\bar{r}_{S2}$) so that numerical accuracy is preserved. After $\hat{x}_s$ is found, the two constant vectors $\hat{y}_{S1}$ and $\hat{y}_{S2}$ may also be calculated since $\hat{n}(t_1)$ and $\hat{n}(t_2)$ have already been found for use in defining $\bar{r}_{S1}$ and $\bar{r}_{S2}$.

The final quantity involving ephemeris data is the satellite angular speed ω arising in (Eq. 13), (Eq. 14), (Eq. 15), and (Eq. 18). As will be seen in Section 1.3.4, it is more convenient to concentrate on the expression $\omega\cdot(t_2 - t_1)$. Notice that, since the typical orbit period is approximately 100 minutes and $(t_2 - t_1)$ ≈ 1 minute, $\omega\cdot(t_2 - t_1)\approx 6\text{x}10^{-2}$ so that the small angle approximation

$$\sin\omega(t_2 - t_1) \approx \omega(t_2 - t_1)$$

Eq. 36

may be used to evaluate $\omega\cdot(t_2 - t_1)$. Also observe that

$$\left|\bar{r}_{s2} \times \bar{r}_{s1}\right| = \sin\omega(t_2 - t_1)\ \left|\bar{r}_{s1}\right|\ \left|\bar{r}_{s2}\right|$$

Eq. 37

Thus, it is found that

$$\omega(t_2 - t_1) \approx \frac{\left|\bar{r}_{s2} \times \bar{r}_{s1}\right|}{\left|\bar{r}_{s1}\right|\ \left|\bar{r}_{s2}\right|}$$

Eq. 38

1.3.2 Alignment adjustments

For perfect alignment, a beam direction is specified by (Eq. 21) and (Eq. 22) where ψ= 45°. There are several types of errors that require these equations to be modified. First, the satellite may yaw, pitch, or roll so that a satellite fixed reference frame may deviate from the directions of the vectors $\hat{x}_s$, $\hat{y}_s$ and $\hat{n}$. Second, the radiometer may not be perfectly aligned with the satellite frame so that even the satellite fixed frame is not adequate. These two kinds of errors may be combined to yield an effective yaw, pitch, and roll that will describe the instrument frame with respect to $\hat{x}_s$, $\hat{y}_s$ and $\hat{n}$. Another class of errors arises from deviations from nominal values within the radiometer itself. Thus, the cone angle may be off-set by δψ from its nominal value. Also, the nominal start angle of 198.4° (see (Eq. 22)) may be shifted.

It will be assumed here that all of these errors are small so that the small angle (first order) approximation may be made in computing trigonometric functions. This assumption has the consequence that yaw, pitch, and roll are commuting motions. Further, a fixed error in the nominal start angle will not be distinguishable from a yawing motion of the satellite. Hence, it will be combined with the yaw error. Thus, there will be four alignment parameters to be found from pre-launch measurements and/or analysis of in-flight data. These are the cone angle offset δψ and the yaw (ϕ_E), pitch (θ_E), and roll (ψ_E). The latter three angles are shown in Figure 5.

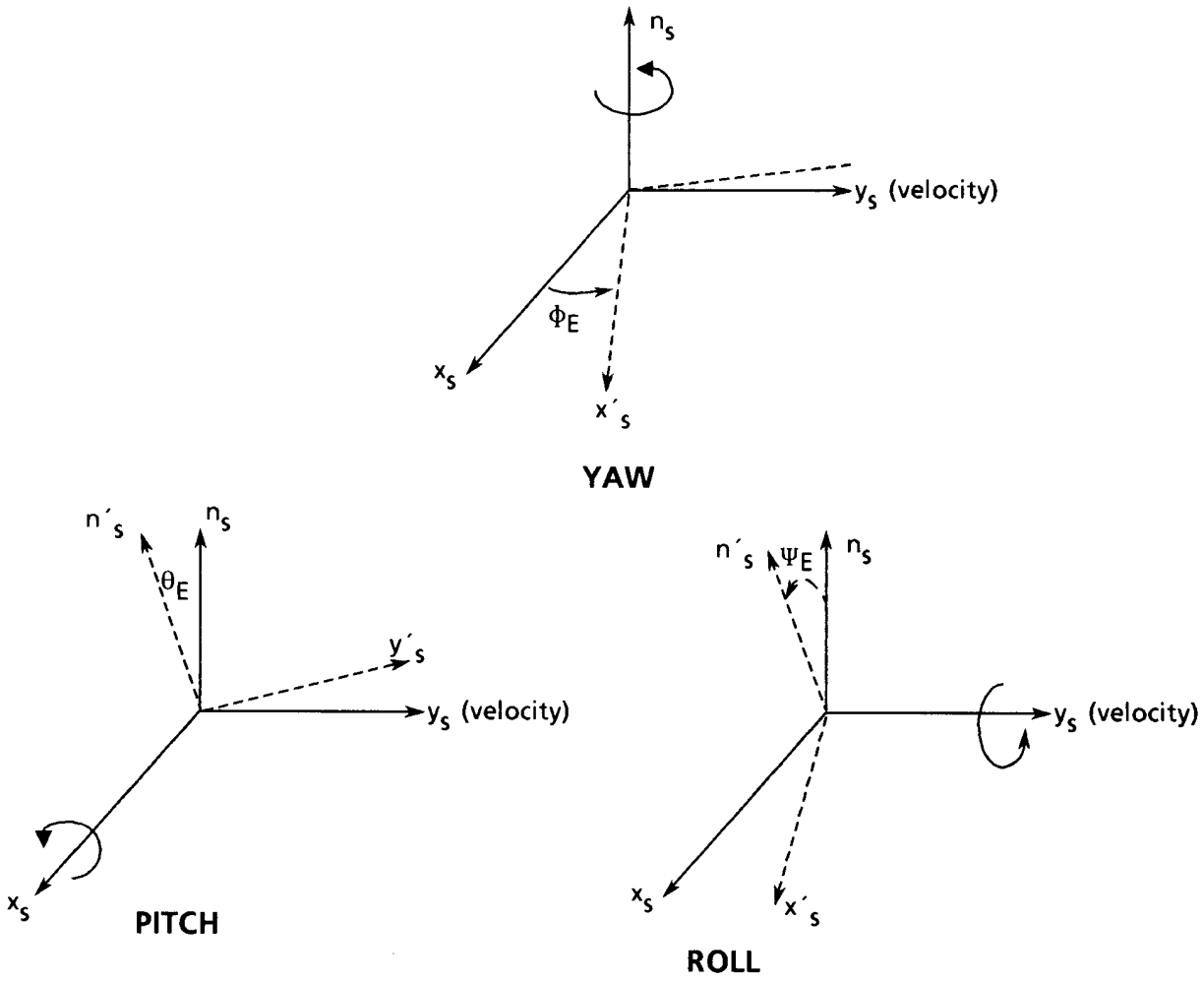

Figure 5. Yaw, Pitch, and Roll Angles

A yaw is described in terms of the matrix

$$D = \begin{pmatrix} \cos\phi_E & \sin\phi_E & 0 \\ -\sin\phi_E & \cos\phi_E & 0 \\ 0 & 0 & 1 \end{pmatrix} \approx \begin{pmatrix} 1 & \phi_E & 0 \\ -\phi_E & 1 & 0 \\ 0 & 0 & 1 \end{pmatrix}$$

Eq. 39

which transforms the components of a vector in the $\hat{x}_s$, $\hat{y}_s$ and $\hat{n}$ coordinate system to the components in a coordinate system fixed within the instrument. Similarly, a pitching motion is described by

$$C \approx \begin{pmatrix} 1 & 0 & 0 \\ 0 & 1 & \theta_E \\ 0 & -\theta_E & 1 \end{pmatrix}$$

Eq. 40

while a roll is described

$$B \approx \begin{pmatrix} 1 & 0 & -\psi_E \\ 0 & 1 & 0 \\ \psi_E & 0 & 1 \end{pmatrix}$$

Eq. 41

A compound motion is described by

$$A = BCD$$

Eq. 42

where second and higher order terms in the angles are to be ignored.

In the instrument fixed coordinate system, the vector gives the beam direction

$$\begin{pmatrix} \sin(\psi+\delta\psi)\cos\phi_s \\ \sin(\psi+\delta\psi)\sin\phi_s \\ -\cos(\psi+\delta\psi) \end{pmatrix} \approx \begin{pmatrix} \sin\psi\cos\phi_s + \delta\psi\cos\psi\cos\phi_s \\ \sin\psi\sin\phi_s + \delta\psi\cos\psi\sin\phi_s \\ -\cos\psi + \delta\psi\sin\psi \end{pmatrix}$$

Eq. 43

Transforming to the $\hat{x}_s$, $\hat{y}_s$ and $\hat{n}$ coordinate frame by means of the matrix A^{-1}, it is found that

$$\begin{aligned} &+\left[-(1-\delta\psi)\cos\psi - \psi_E\cos\psi\cos\phi_s + \theta_E\sin\psi\sin\phi_s\right]\hat{n}_s(t) \\ &+\left[(1+\delta\psi)\sin\psi\sin\phi_s + \phi_E\cos\psi\cos\phi_s - \theta_E\cos\psi\right]\hat{y}_s(t) \\ \hat{s} &= \left[(1+\delta\psi)\cos\psi\cos\phi_s - \phi_E\sin\psi\sin\phi_s - \psi_E\cos\psi\right]\hat{x}_s \end{aligned}$$

Eq. 44

where use has been made of the fact that $\cos\psi = \sin\psi$ for $\psi = 45°$.

Numerically since ϕ_s is a known function of $t\text{-}t_s$ (see (Eq. 22)), the fastest procedure for evaluating (Eq. 44) is to make use of a stored table of values for $\cos\psi\cos\phi_s$ and $\sin\psi\sin\phi_s$ at times of interest relative to the scan start time t_s. Each of the square brackets in (Eq. 44) can be reevaluated any time the alignment parameters are updated.

1.3.3 Reference height correction

Certain of the SSMIS beams are to be referenced to heights other than the Earth's surface. As was shown in Section 1.2, an exact solution of the problem is too complicated to be used in an operational algorithm. However, a very simple correction results if the Earth is treated as flat in the immediate vicinity of the point where the beam intersects the Earth. For a flat Earth, as is evident from Figure 6,

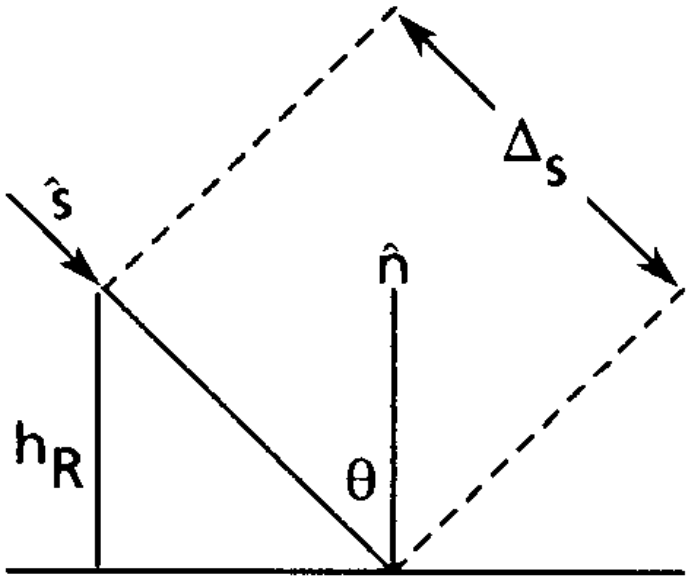

Figure 6. Approximate Calculation of Reduction in Slant Range

the slant range for a beam referenced to a height h_R is reduced compared to that for a beam intersecting the surface by an amount

$$\Delta s = h_R / \cos\theta$$

Eq. 45

where θ is the angle of incidence. An approximate determination of cosθ will be discussed below. But first, assuming that it is known, the derivation of the beam latitude and longitude equations will be completed. Using (Eq. 45), (Eq. 32) becomes

$$\bar{r}_b = \bar{r}_s + (s - \Delta s)\ \hat{s}\ - h_R\ \hat{n}_b$$

Eq. 46

where s is the slant range to the surface given by (Eq. 24). A simplification of (Eq. 46) results if the unit normal n_b is approximated as

$$\hat{n}_b \approx \bar{r}_b / |\bar{r}_b|$$

Eq. 47

With this expression, it is found that

$$\bar{r}_b \approx \left[\bar{r}_s + (s - \Delta s)\hat{s}\right] / \left[1 + h_R / |\bar{r}_b|\right]$$

Eq. 48

The remaining computation now reverts to the ellipsoidal Earth model. Recalling (Eq. 28) and (Eq. 29), it is seen that the factor $[1+h_r / |\bar{r}_b|]$ in (Eq. 48) will cancel in computing the beam latitude and longitude. It may be ignored. Thus, simply by reducing the slant range to the surface by (Eq. 45), the computation of latitude and longitude for a reference height h_R is achieved.

The reference height correction procedure will be completed when a rule for calculating cosθ in (Eq. 45) is specified. For this computation, one may approximate the Earth by a sphere with radius R. Then, the law of sines implies (see Figure 7) that

$$\sin\theta = \frac{h+R}{R}\sin\psi$$

Eq. 49

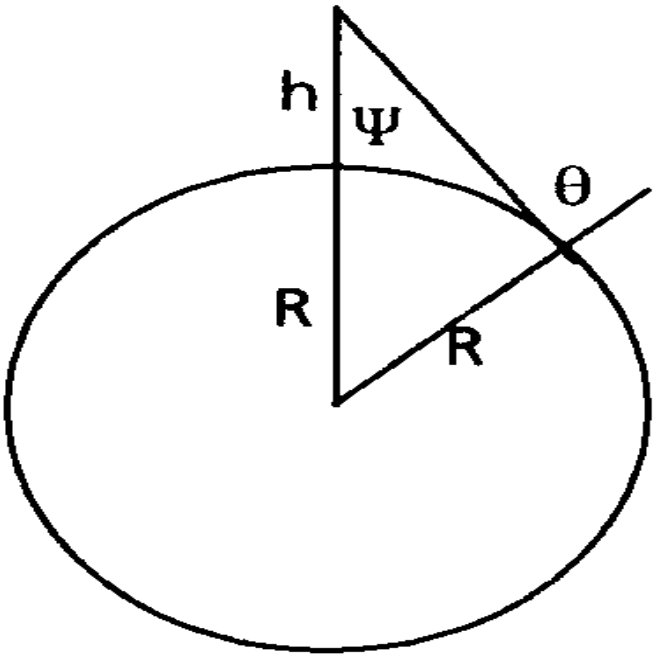

Figure 7. Approximate Angle of Incidence Calculation

This equation shows that θ depends on the satellite altitude h (which has a nominal value h_o = 833 km, but may vary) and the angle ψ (which is nominally ψ_o = 45° but, as discussed in Section 1.3.2, may be perturbed). Differentiating (Eq. 49) shows that

$$\cos\theta_0 d\theta = \frac{\sin\psi_0}{R} dh + \frac{h_0+R}{R}\cos\psi_0 d\psi$$

Eq. 50

Thus

$$\cos\theta \approx \cos\theta_0 - \sin\theta_0 d\theta = \cos\theta_0 - \frac{\tan\theta_0 \sin\psi_0}{R} dh - \frac{h_0+R}{R}\tan\theta_0 \cos\psi_0 d\psi$$

Eq. 51

Now (Eq. 44) shows how to calculate $\cos\psi_o d\psi$:

$$-(\hat{s})_n = \cos\psi \approx \cos\psi_0 - \sin\psi_0 d\psi$$

Eq. 52

or

$$\cos\psi_0 d\psi = \frac{\cos\psi_0 + (\hat{s})_n}{\tan\psi_0}$$

Eq. 53

Also dh = h-833 km. If the Earth radius in (Eq. 51) is approximated by the true radius at 45° latitude (R= 6367.521 km) and h is approximated as the average of the heights at the two ephemeris times t_1 and t_2 (see (Eq. 11)), then it is found that

$$\cos\theta = .600519 - 1.47865\times10^{-4}\left\{\left[h(t_1) + h(t_2)\right]/2 - 833\right\} - 1.50572\left[\cos 45 + (\hat{s})_n\right]$$

Eq. 54

1.3.4 Base point location

Base point latitudes and longitudes are given by (Eq. 28) - (Eq. 31) with $\bar{r}_b$ given by (Eq. 23). In (Eq. 23), s is either the range to the surface (see (Eq. 24)) or the range reduced by (Eq. 45) if the reference height is greater than zero. The computation of the components of s has been discussed in Section 1.3.2 assuming $\hat{x}_s$, $\hat{y}_s(t)$ and $\hat{n}(t)$ were known. The ephemeris data determine $\hat{x}_s$ (Section 1.3.1). Thus, only the evaluation of (Eq. 14), (Eq. 15), and (Eq. 18) need be considered.

The form is the same in each case and involves the functions $[\sin\omega(t-t_2)]/[(\sin\omega(t_2-t_1)]$ and $[\sin\omega(t-t_1)]/(\sin\omega(t_2-t_1)]$. For a fast algorithm, it is not desirable to calculate these transcendental functions directly. Instead, making use of the observation, already made in Section 1.3.1, that the maximum argument of the trigonometric functions is small, these functions may be expanded as

$$s_{r1} = -\frac{\sin\omega(t-t_2)}{\sin\omega(t_2-t_1)} = -\frac{t-t_2}{t_2-t_1}\left[1 - \frac{\omega^2(t_2-t_1)^2}{6}\left\{\left(\frac{t-t_2}{t_2-t_1}\right)^2 - 1\right\}\right]$$

Eq. 55

and

$$s_{r2} = \frac{\sin\omega(t-t_1)}{\sin\omega(t_2-t_1)} = \frac{t-t_1}{t_2-t_1}\left[1 - \frac{\omega^2(t_2-t_1)^2}{6}\left\{\left(\frac{t-t_1}{t_2-t_1}\right)^2 - 1\right\}\right]$$

Eq. 56

where quadratic and higher powers of ω are ignored. (Eq. 38) shows that

$$\omega_t = \frac{\omega^2}{6}(t_2 - t_1)^2 = \frac{|\bar{r}_{s2} \times \bar{r}_{s1}|^2}{6|r_{s2}|^2 |r_{s1}|^2}$$

Eq. 57

so that, defining

$$\omega_t' = \omega_t + 1$$

Eq. 58

$$t_{m1} = (t - t_1) / (t_2 - t_1)$$

Eq. 59

$$t_{m2} = (t - t_2) / (t_2 - t_1) = t_{m1} - 1$$

Eq. 60

it is found that

$$s_{r1} = -(\omega_t' - \omega_t t_{m2}^2) t_{m2}$$

Eq. 61

$$s_{r2} = (\omega_t' - \omega_t t_{m1}^2) t_{m1}$$

Eq. 62

Thus, the algebraic approximations

$$\bar{r}_s(t) = s_{r1}\bar{r}_{s1} + s_{r2}\bar{r}_{s2}$$

Eq. 63

$$\hat{n}(t) = s_{r1}\hat{n}_1 + s_{r2}\hat{n}_2$$

Eq. 64

$$\hat{y}_s(t) = s_{r1}\hat{y}_{s1} + s_{r2}\hat{y}_{s2}$$

Eq. 65

are found for (Eq. 15), (Eq. 14) and (Eq. 18) respectively. Of course t in (Eq. 59)-(Eq. 65) must correspond to one of the times defining a base point.

1.3.5 Interpolation between basepoints

In order to save computation time, only a few base points will be located precisely. Thus, an interpolation scheme is required to locate the remainder of the beams. If interpolation is accomplished by polynomials, as will be done here, it is desirable to keep the degree of the polynomials as low as possible for speed in

evaluation. Unfortunately, acceptable accuracy over the full range of scan angles cannot be achieved in this fashion if only a single polynomial is used. By dividing the range of antenna scan angles into a number of sections, each containing only four base points, it is possible to meet accuracy requirements while confining our attention to third degree polynomials. This is a good compromise between accuracy and speed requirements and was used in the SSM/I location algorithm.

Thus, consider the problem of approximating a function f(x) in the interval $-1 \le x \le 1$ by the third degree polynomial

$$P(x) = p_o + p_1 x + p_2 x^2 + p_3 x^3$$

Eq. 66

where P(x) agrees with f(x) at the four points x_1, x_2, x_3, and x_4 . For the problem at hand, x represents the normalized antenna scan angle ϕ_s (scaled, of course, so that x is in the prescribed interval), the points x_1, x_2, x_3, and x_4 are the normalized scan angles corresponding to the positions of the base points, and f(x) with its corresponding P(x) is either the beam latitude or longitude. The connection between the physical antenna scan angle ϕ_s and the normalized variable x is given by the relations

$$x = \frac{2}{\phi_{sb} - \phi_{sa}} \left(\phi_s - \phi_{sa} \right) - 1$$

Eq. 67

$$\phi_s = \frac{\phi_{sb} - \phi_{sa}}{2} x + \frac{\phi_{sb} + \phi_{sa}}{2}$$

Eq. 68

where it is assumed that the angle ϕ_s lies in the interval $\phi_{sa} \le \phi_s \le \phi_{sb}$.

1.3.5.1 Choice of base points

A question arises concerning the best choice of the points x_i (i=1,...4). A simple strategy is the choice of equally spaced points. However, this may not be optimal. It is shown in many texts on numerical analysis that the error in the approximation (Eq. 66) may be expressed as

$$f(x) - P(x) = \frac{f^{(4)}(\xi(x))}{4!} \Pi(x)$$

Eq. 69

Where

$$\Pi(x) = (x - x_1)(x - x_2)(x - x_3)(x - x_4)$$

Eq. 70

Here $f^{(4)}$ is the fourth derivative of f evaluated at some point ξ (which depends on x) in the interval ($-1<\xi<1$). Since the function f is not under our control, the best strategy for achieving high accuracy is to minimize the maximum (over x) of the function $|\Pi(x)|$. It is well known that the solution of this problem

is to choose x_i (i=1,...,4) as the roots of the fourth degree Chebychev polynomial of the first kind. Unfortunately, all of these roots lie in the interior of the interval $(-1 \le x \le 1)$ so that four base points will have to be computed in each section. Since a base point computation is expensive in terms of computer time, it would be desirable to make multiple use of at least some of the base points. This is accomplished by demanding that the two extreme points in each section lie at the extremes of the interval; i.e., $x_1 = -1$ and $x_4 = 1$. In this way, these two base points may be used for two separate sections. Thus, only the two points x_2 and x_3 remain to be chosen. Clearly, there is symmetry about the point x=0 so that $x_3 = -x_2$. Thus, the problem becomes one of choosing x_2 so as to minimize the function $\max_{(x)}\{|(x^2-1)(x^2-x_2^2)|\}$ with respect to x_2. It may be shown that the solution is

$$x_2 = -\sqrt{3-\sqrt{8}} = -.4142135621...$$
$$x_3 = \sqrt{3-\sqrt{8}}$$

Eq. 71

With these choices for x_i (i=1...4), $\max_{(x)}\{|\Pi(x)|\} = .17157$ over the interval $-1 \le x \le 1$. This is roughly 15% smaller than would be achieved if the equal spacing choice $x_2 = -1/3$, $x_3 = 1/3$ were made. Of course, the full 15% will not necessarily be realized in the reduction of the error of the approximation for f because the factor $f^{(4)}$ in (Eq. 69) may vary with x. Nevertheless, as will be shown later, a worthwhile improvement is achieved with no additional calculations in an operational computer program if the choice (Eq. 71) is made.

The question of choosing the appropriate number of sections and their end points remains to be discussed. The simplest scheme is to divide the full scan into N_{sect} sections, each occupying equally sized azimuthal angle intervals and whose end points coincide with one of the basic beam positions. Since there will be four base points per section, a total of $N_{bse} = 3\ N_{sect} + 1$ base points will be necessary (recall that base points bounding sections will be common to two sections, except for the first and last). Since a full scan contains 180 basic beam positions, the choice

$$N_{pts} = \left\{ \begin{array}{l} \dfrac{180}{N_{sect}} \ \text{(in section 1)} \\ \dfrac{180}{N_{sect}} \ \text{(in sections } 2, 3, ...) \end{array} \right\}$$

Eq. 72

is made for the number of points N_{pts} in each section (including end points, thus counting bounding points twice). The increment in the normalized azimuthal angle change Δu between basic beam positions is

$$\Delta u = \left\{ \begin{array}{l} \dfrac{2}{N_{pts}-1} \ \text{(in section 1)} \\ \dfrac{2}{N_{pts}} \ \text{(in sections } 2, 3, ...) \end{array} \right\}$$

Eq. 73

Because N_{pts} is an integer, the possibilities shown in Table I occur.

Table I. Possible Divisions of a Scan into Sections

N_{sect}	N_{bse}	N_{pts}	Δu
2	7	90,91	2/89 , 2/90
3	10	60,61	2/59 , 2/60
4	13	45,46	2/44 , 2/45
5	16	36,37	2/35 , 2/36
6	19	30,31	2/29 , 2/30
9	28	20,21	2/19 , 2/20
10	31	18,19	2/17 , 2/18
12	37	15,16	2/14 , 2/15
.	.	.	.
.	.	.	.
.	.	.	.

The trade-off between these possibilities is accuracy vs computer time. Later, it will be seen that it is useful to choose a different number of sections for the polar regions than for the remainder of the Earth. The choices $N_{sect} = 9$ for the polar regions and $N_{sect} = 3$ elsewhere are suitable for the SSMIS.

1.3.5.2 Computation of interpolated latitude and longitude

Consider the evaluation of (Eq. 66) for $x = u_1$, $u_2 = u_1 + \Delta u$, $u_3 = u_1 + 2\Delta u$, . . . where $u_1 = -1$. Substituting $u_{i+1} = u_i + \Delta u$ in (Eq. 66) shows that

$$P(u_{i+1}) = P(u_i) + Q(u_i)$$

Eq. 74

where

$$Q(u) = \left[3p_3 \Delta u\right]u^2 + \left[3p_3 (\Delta u)^2 + 2p_2 \Delta u\right]u + \left[p_3 (\Delta u)^3 + p_2 (\Delta u)^2 + p_1 \Delta u\right]$$

Eq. 75

Similarly, it is found that

$$Q(u_{i+1}) = Q(u_i) + R(u_i)$$

Eq. 76

where

$$R(u) = \left[6p_3(\Delta u)^2\right]u + \left[6p_3(\Delta u)^3 + 2p_2(\Delta u)^2\right]$$

Eq. 77

likewise

$$R(u_{i+1}) = R(u_i) + A$$

Eq. 78

where

$$A = 6p_3(\Delta u)^3$$

Eq. 79

(Eq. 74), (Eq. 76), and (Eq. 78) form a recursive set of equations where each new value of P is found by only three additions after initial values $P(u_1)$, $Q(u_1)$ and $R(u_1)$ are specified. This is substantially better than the three multiplications and three additions necessary for a straightforward evaluation of (Eq. 66).

Suppose that the function f(x) that is approximated by P(x) has known values y_1, y_2, y_3, and y_4 (the base point values) when x= x_1, x_2, x_3, and x_4 respectively. Then

$$\begin{aligned} P(u_1) &= y_1 \\ Q(u_1) &= q_3(\Delta u)^2 + q_2\Delta u + q_1 + B \\ R(u_1) &= 6q_3(\Delta u)^2 + 2q_2\Delta u - 6q_3\Delta u \end{aligned}$$

Eq. 80

where

$$q_i = p_i \Delta u \qquad (i = 1,2,3)$$

Eq. 81

and

$$B = 3q_3 - 3q_3\Delta u - 2q_2$$

Eq. 82

To complete the specifications, a rule for calculating p_i or, equivalently, q_i for i= 1,2,3 must be given in terms of the function values y_i (i=1…4) at the points x_i (i=1…4). The standard representation of P(x) in terms of the Lagrange polynomials may be expanded to yield

$$p_1 = \frac{1}{2(1-x_2^2)}\left[x_2^2 y_1 + \frac{y_2}{x_2} - \frac{y_3}{x_2} - x_2^2 y_4 \right]$$

$$p_2 = \frac{1}{2(1-x_2^2)} \quad y_1 - y_2 - y_3 + y_4$$

$$p_3 = \frac{1}{2}(y_4 - y_1) - p_1$$

Eq. 83

Thus, defining

$$V = \frac{\Delta u}{2}(y_4 - y_1)$$

Eq. 84

it is found that

$$q_1 = \frac{\Delta u}{2x_2\ (1-x_2^2)} \quad (y_2 - y_3) - \frac{x_2^2}{(1 - x_2^2)} \quad V$$

$$q_2 = \frac{\Delta u}{2\,(1-x_2^2)} \quad (y_1 + y_4 - y_2 - y_3)$$

$$q_3 = V - q_1$$

Eq. 85

1.4 Accuracy

A beam location algorithm based on the discussion in Section 1.3 has been developed for the SSMIS software package. It is implemented by a driver subroutine named LOCATE, a subroutine EPHEM to calculate quantities that do not change between the two ephemeris times t_1 and t_2, a subroutine BASEPT to perform the base point location calculations, and a subroutine INTERP to perform the polynomial interpolations. A number of tests have been performed using these routines to verify that performance specifications will be met. These tests were performed for an assumed circular orbit with an inclination angle of 98.7°. In most of the cases, the satellite altitude was chosen to be 833 km above the Earth at 45° latitude. Of course, the flattening of the Earth towards the poles implies that the height above the surface will vary with latitude. Unless explicitly stated below, this is the orbit that is being considered. A plot of the subsatellite track showing beam coverage is presented in Figure 8. In all cases to be discussed below, "errors" refer to differences between exact computations, (performed with the equations in Section 1.2 using the exact circular orbit location at a time of interest and involving none of the approximations discussed in Section 1.3), and the use of the approximations discussed in Section 1.3.

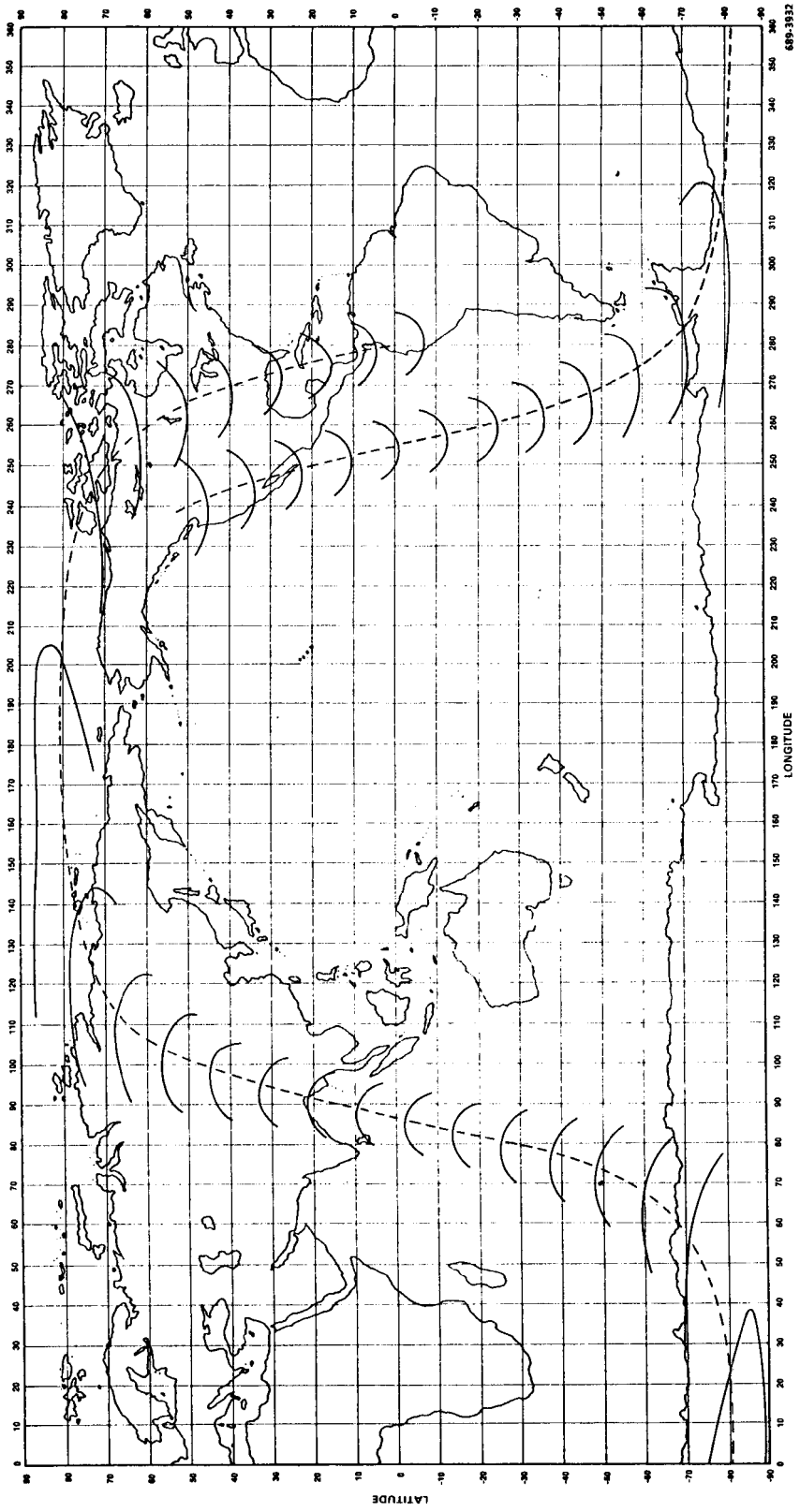
LONGITUDE
LATITUDE
689-3932

Figure 8. Sample Subsatellite Track and SSMIS Beam Coverage

The first test performed was a check on the accuracy of the base point locations. Calculations showed that the maximum base point location error was less than 0.2 km. If, as in the SSM/I algorithm, a linear approximation (equivalent to setting $\omega_t = 0$ instead of using (Eq. 57)) had been made, the maximum error in the base point location would have been 4 km. This order of magnitude improvement, obtained at little cost, helps reduce the subsequent interpolation errors considerably.

The extremely low base point location errors cannot be maintained when interpolating with only a few base points. The shapes of the scan lines shown in Figure 8 indicate that, for a fixed number of base points, the interpolation error should grow towards the polar regions. Further, because of the larger azimuthal scan range for the SSMIS compared to the SSM/I, the interpolation error problem should be expected to be more severe. This is indeed the case. Computations showed a maximum location error of 7.3 km when using $N_{sect} = 6$ sections ($N_{bse} = 19$ base points) for locating a beam at the Earth's surface. This occurred near the South Pole. The next possible value for N_{sect} is 9 (see Table I in Section 1.3.5.1) which implies $N_{bse} = 28$. With this choice, the maximum beam location error is 2.7 km at the surface and is well within the required 7-km accuracy. The error decreases rapidly towards lower latitudes.

In order to reduce computation time, it is not desirable to use 28 base points at all latitudes. For this reason, the cases $N_{sect} = 2$ and $N_{sect} = 3$ were investigated. $N_{sect} = 2$ yielded a maximum beam location error at the surface of 4 km below 60° latitude but this error increased rapidly between 60 and 70° latitude. To obtain a more balanced error curve, the choice $N_{sect} = 3$ was made. It was found that with $N_{sect} = 3$, the maximum location error was 2.6 km below 72° latitude. Thus, the choice $N_{sect} = 9$ polewards of 72° and $N_{sect} = 3$ otherwise was made. The resultant maximum error curve for locating the beam at the surface is shown in Figure 9. It shows that the maximum location error depends on whether the satellite is approaching or departing the polar regions. This is not surprising in view of the shapes of the scan line shown in Figure 8. The discontinuity near 72° is the result of the change in the number of sections used. Its precise location will vary slightly from orbit to orbit since the changeover point is keyed to the bounding subsatellite latitudes at the times t_1 and t_2 used in the algorithm. This transition is chosen so that if any subsatellite points between the ephemeris times t_1 and t_2 is polewards of 72° latitude, the 9-section division of a scan is used. Thus, in some cases, the maximum immediately to the equator side of 72° will be considerably less than the 2.6 km shown because the 9-section curve will be followed.

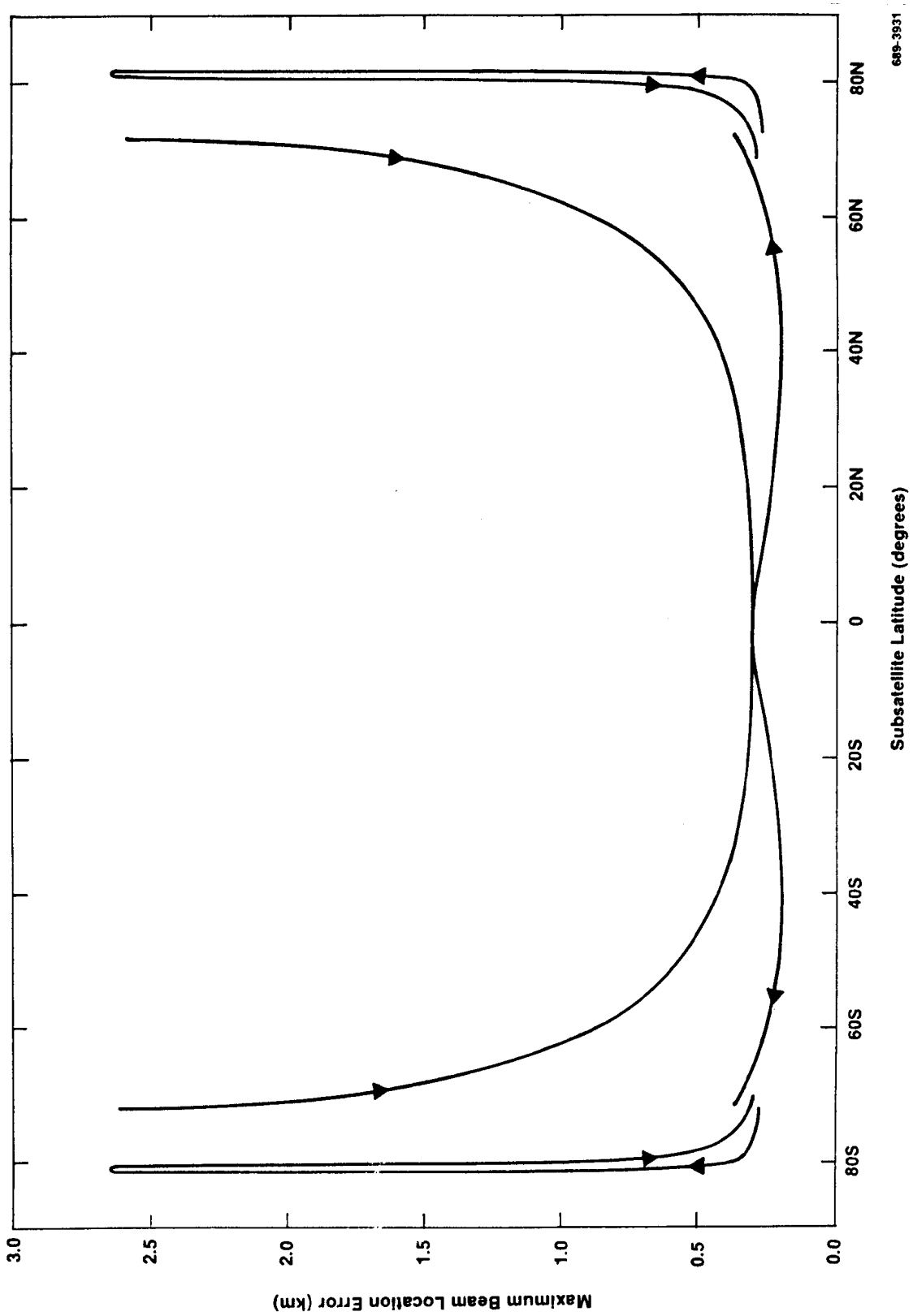
Maximum Beam Location Error (km)
3.0
2.5
2.0
1.5
1.0
0.5
0.0
80S
60S
40S
20S
0
20N
40N
60N
80N
Subsatellite Latitude (degrees)
689-3931

Figure 9. Maximum SSMIS Beam Location Error at Earth's Surface (Nominal 833 Km Orbit)

A test was made to compare the accuracy of using the recommended base point azimuthal spacing versus an equal spacing choice (see Section 1.3.5.1). For the $N_{sect} = 3$ region, it was found that the maximum error in each scan using equal spacing was typically 8-10% larger than the recommended algorithm. In the $N_{sect} = 9$ region, the worst case errors near the orbit extremes were also increased by this amount although closer to the transition point at 72°, where the errors are order of magnitude smaller, the equal spacing choice yielded smaller errors than the recommended algorithm.

The tests of the algorithm for a reference height of 11 km revealed that the maximum beam location error would be less than 2.1 km. This is less than the error for the surface location and is to be expected on the basis of the curves shown in Figure 9. Locating a beam at 11 km near the poles implies that the scan curves will have a truncated range. Hence, third degree polynomials will not have to cover such a wide variation in position.

Tests for non-ideal orbital heights showed that location errors decrease compared to the maximum of less than 2.7 km if the orbit height is decreased from the nominal 833 km. For a 770-km orbit, the maximum location error at the surface is less than 1.5 km. This is due to the truncated range of the scan curves caused by the lower orbit. In the other direction, location errors are increased due to the extended range of the scan lines. Maximum errors for the surface location increase to 2.72 km for an 860-km orbit and to 4.98 km for an 880-km orbit. Of course, it is expected that these extreme orbital altitude excursions will not occur in practice.

[End of Appendix A]